

Mechanism of intercalation and deintercalation of lithium ions in graphene nanosheets

TIAN LeiLei¹, ZHUANG QuanChao^{1*}, LI Jia¹, SHI YueLi¹, CHEN JianPeng¹, LU Feng¹ & SUN ShiGang²

¹ School of Materials Science and Engineering, China University of Mining & Technology, Xuzhou 221116, China;

² State Key Laboratory of Physical Chemistry of Solid Surfaces, Department of Chemistry, College of Chemistry and Chemical Engineering, Xiamen University, Xiamen 361005, China

Received January 13, 2011; accepted March 2, 2011

Graphene nanosheets (GNSs) were synthesized by reducing exfoliated graphite oxides. Their structure, surface morphology and lithium storage mechanism were characterized and investigated systematically using X-ray diffraction, atomic force microscopy, scanning electron microscopy, charge-discharge tests, cyclic voltammetry and electrochemical impedance spectroscopy. It was found that the GNSs, which were obtained via chemical synthesis, were primarily less than 10 graphene layers. The GNS electrodes, which were fabricated from the reduced GNSs, exhibited an enhanced reversible lithium storage capacity and good cyclic stability when serving as anodes in lithium-ion batteries. Also, the first-cycle irreversible capacities of the system were relatively high, because of the formation of a solid electrolyte interphase film on the surface of the GNS electrode and the spontaneous stacking of GNSs during the first lithiation. The electrochemical impedance spectroscopy results suggest that the solid electrolyte interphase film on the GNS electrode during first lithiation were primarily formed at potentials between 0.95 and 0.7 V. Also, the symmetry factor of the charge transfer was measured to be 0.446.

lithium-ion batteries, graphene, solid electrolyte interphase film, electrochemical impedance spectroscopy

Citation: Tian L L, Zhuang Q C, Li J, et al. Mechanism of intercalation and deintercalation of lithium ions in graphene nanosheets. *Chinese Sci Bull*, 2011, 56: 3204–3212, doi: 10.1007/s11434-011-4609-6

Graphene is a flat monolayer of sp^2 -hybridized carbon atoms tightly packed in a two-dimensional honeycomb lattice [1]. Recent research has shown that graphene exhibits many unusual electronic, thermal, structural, and mechanical behaviors. Also, it has high specific surface areas (over $2600 \text{ m}^2 \text{ g}^{-1}$), and fascinating transport phenomena such as a room-temperature quantum Hall effect, an ambipolar electric-field effect, and ballistic conduction of charge carriers [2–8]. Partoens et al. [9] found that the electronic structure of few-layer graphene (number of layers less than 10) is different from that of bulk graphite. Because of this, it is useful to define three different types of graphene: single-layer graphene (SG), bilayer graphene (BG), and few-layer graphene (FG, number of layers ≤ 10) [10].

These properties make graphene very promising for many applications such as solar cells, sensors, supercapacitors, and hydrogen storage. Despite optimistic expectations for graphene-based electronics, it seems unlikely that they will become commonplace within the next two decades. In the meantime, many other graphene-based applications are coming of age. One of these exciting possibilities is using bulk graphene powders as anode materials for reversible lithium storage in lithium-ion batteries (LIB) [11,12]. Because of its large surface-to-volume ratio and highly conductive nature, graphene may have properties that make it more suitable than graphite for reversible lithium storage in lithium-ion batteries. This is because lithium ions could be bound not only on both sides of the graphene sheets, but also at the edges and covalent sites of the graphene nanoplatelets. Its theoretical capacity ($740\text{--}780 \text{ mA h g}^{-1}$) is

*Corresponding author (email: zhuangquanchao@126.com)

more than two times of that of bulk graphite. Therefore, we expect that graphene could overtake its 3D counterpart (graphite) for enhanced Li storage in LIB. In addition, when graphene is used as an anode material, the diffusion of the lithium-ions is much easier. Thus, the rate capability is significantly enhanced. However, as an anode material, graphene has two disadvantages. First, graphene sheets are prone to stack into multilayer structures. Thus they lose their high specific surface areas and intrinsic properties. Second, there is a rather large irreversible capacity in the first charge-discharge cycle, because of the subsequent loss in surface areas. An explanation of the mechanism of intercalation-deintercalation of the lithium ions in the graphene is important for solving these problems. However, currently, no explanation has been put forth.

In this work, graphene nanosheets (GNSs) were synthesized by reducing exfoliated graphite oxides. Their structure, surface morphology and lithium storage mechanisms were characterized and investigated systematically using X-ray diffraction (XRD), atomic force microscopy (AFM), field-emission scanning electron microscopy (FE-SEM), charge-discharge tests and cyclic voltammetry (CV). The first lithiation process of the GNSs was studied using electrochemical impedance spectroscopy (EIS), and the variation in the impedance with decreasing electrode polarization potential was analyzed.

1 Experimental

1.1 Preparation of the GNSs

Graphene oxide was prepared from natural graphite powder via the modified Hummers method [11,13]. The obtained graphite oxide was re-dispersed in DI water. The exfoliation of the graphite oxide to nanosheets was achieved through ultrasonication of the dispersion using an Ultrasonic Instrument (FS-600, Shanghai Sonxi Ultrasonic Instrument Co. Ltd., Shanghai, China). In the procedure for the chemical conversion of graphite oxide to graphene [14], the resulting homogeneous dispersion was poured into a round-bottomed flask, to which hydrazine monohydrate solution (reducing agent) was subsequently added. An ammonia solution was used to adjust the pH value of the solution to 10. After being refluxed at 100°C for 2 h, the suspension gradually changed to a dark black color as the GNS dispersion was formed. The suspension was filtered to produce a fluffy graphene cake. The graphene cake was dried to obtain a bulk GNS powder. Finally, GNSs obtained using chemical reduction were heat treated at 500°C in a nitrogen atmosphere for 2 h to remove the -H and -OH groups.

1.2 Nanostructural and physical characterizations

The structures of GNSs were analyzed using XRD (Bruker AXS D76181 X-ray diffractometer, Karlsruhe, Germany)

and FE-SEM (JEOL 6701F, Tokyo, Japan). The GNS electrodes were characterized using AFM (Pico Scan 2100, Molecular Imaging Co. Ltd., Tempe, AZ, USA).

1.3 Electrochemical testing of GNS electrodes

The graphene electrodes used in this study were prepared by spreading a mixture of 80% GNS powder and 20% polyvinylidene fluoride (Kynar FLEX 910, Elf Atochem, Issaquah, WA, USA) binder dissolved in *N*-methyl pyrrolidone (Fluka Inc., St. Louis, MO, USA) onto a Cu foil (thickness: 20 μm) current collector. The electrolyte consisted of 1 mol L⁻¹ LiPF₆ in a mixture of ethylene carbonate (EC), dimethyl carbonate (DMC), and diethyl carbonate (1:1:1, weight ratio, Guotaihuarong Co., Zhangjiagang, China).

The charge-discharge experiments were conducted in a two-electrode button cell using a Li foil (99.9%, China Energy Lithium Co., Ltd., Tianjin, China) as a counter electrode. The cells were galvanostatically charged and discharged at a current density of 100 mA g⁻¹ over a range of 0–3 V. The CV and EIS measurements were performed in a three-electrode glass cell with Li foils serving as both the auxiliary and reference electrodes in an electrochemical work station (CHI 660C, Chenhua Co., Shanghai, China). The CV curves were measured at 1 mV s⁻¹ over the range from 3 to 0 V. The amplitude of the ac perturbation signal was 5 mV and the frequency range was varied from 10⁴ to 10⁻² Hz, and the electrode was equilibrated for 1 h before the EIS measurements to attain steady state conditions.

2 Results and discussion

2.1 XRD analysis

Figure 1 shows the XRD patterns of both the raw graphite and the final products. The sharp peak near 26° can be seen in both samples. This peak is attributed to the (002) planes of carbon materials. However, GNS exhibited a slightly larger *d*₀₀₂ interlayer spacing (3.49 Å) than the raw graphite (3.38 Å). Moreover, the (002) diffraction peak of GNS weakened in intensity and slightly broadened, because of

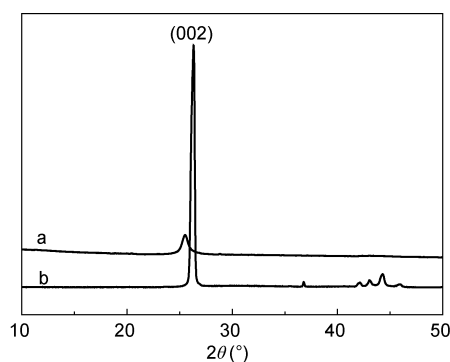


Figure 1 XRD patterns of the (a) graphene and (b) raw graphite.

the short-range ordering in the crystal structure and the existence of defects in the products. This is in accordance with previously reported results [15,16].

2.2 SEM and AFM observation

Figure 2 (a) shows a FE-SEM image of a top-view of the GNSs. From the figure, it can be seen that the layered plates are composed of many curled nanosheets with diameters ranging 10–20 μm . However, in Figure 2 (b), it can be seen that the edges the restacked GNS are made up of finely divided nanoplates with intrinsic ripples. The thickness of an individual stack in the nanoplates was estimated to be 5 nm. This suggests that the self-restacked GNSs consist of several layers, because along their scrolled edge [10,12], the actual thickness of prepared graphene sheets should be much less than 5 nm. Figure 3 shows a 3-D AFM topography image of an individual exfoliated graphene sheet. In this image, the wrinkled and ragged structure of the surface can be seen. Corrugation and scrolling are part of the intrinsic nature of graphene nanosheets. They result from the fact that the 2D membrane structure becomes thermodynamically stable via bending [1,12,17]. Therefore, the GNSs prepared in this work do not exceed 10 layers.

2.3 Charge-discharge test

The charge-discharge curves and cycling performance of the GNS anode are shown in Figures 4 and 5, respectively. From these figures, the charge-discharge behavior over the

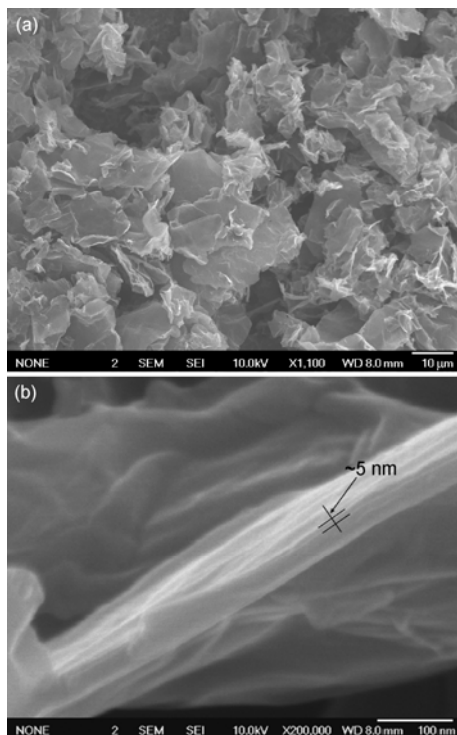


Figure 2 SEM images of the GNS. (a) Top view and (b) edge.

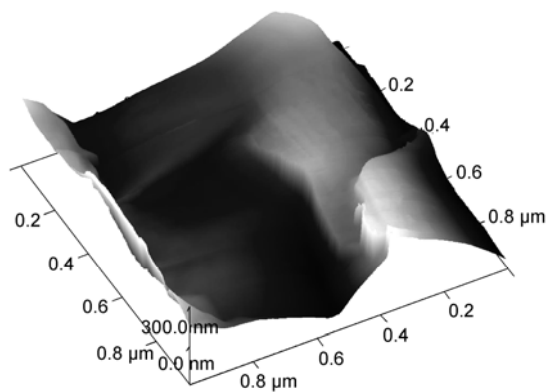


Figure 3 Topographic AFM image of an exfoliated single graphene sheet.

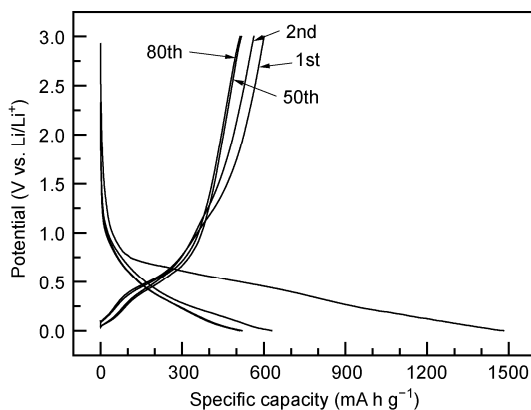


Figure 4 Charge-discharge profiles of the GNS anode at a current density of 100 mA g^{-1} .

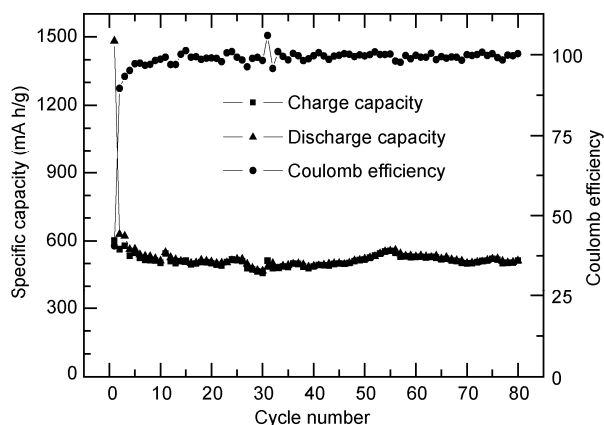


Figure 5 Cycling performance of the GNS anode at a current density of 100 mA g^{-1} .

range 0–3 V can be seen. In the profile, the first cycle discharge and charge capacities of the GNS/Li battery at a current density of 100 mA g^{-1} are 1481.5 and 601 mA h g^{-1} . This greatly exceeds the theoretical capacity of graphite, which is 372 mA h g^{-1} . Nevertheless, the first cycle columbic efficiencies are relatively low (40.6%) and the irreversible capacities are higher. Note that the reversible capacity

from the 2nd cycle is maintained at 85% after 80 cycles.

Figure 6 shows cyclic voltammograms of the GNS anode. The shape of the CV curves matches well with that of the charge-discharge profiles. Two cathodic peaks can be seen during the first lithiation process. The first current peak appeared in voltage range of 0.8–0.4 V and disappeared during subsequent cycles. This can be attributed to the formation of solid electrolyte interphase (SEI) films on the surface of the GNS electrode [18,19]. The irreversible capacity of carbonaceous materials during the first cycle can be primarily associated with the consumption of lithium ions in the course of the reaction with the active sites of the electrode, and the decomposition of electrolytes, which leads to the formation of SEI films on the surface of the electrode [11,15]. This peak can be typically enhanced by increasing the specific surface area and structural disorder of the electrode materials. The second peak is located below 0.2 V, which corresponds to the insertion of Li^+ into the lattice of the GNS electrode. A large voltage hysteresis can be observed during first delithiation process. According to the Li storage model of GNS [20], the reaction of Li with the active defects during the discharge processes occurs at low voltages. However, the breaking of the relatively strong bonds of the Li atom with the defects during the charge processes takes place at high voltages. Thus, resulting in a large voltage hysteresis. After several cycles, the current peaks became stable, which indicates that the insertion-extraction of Li^+ produces good reversibility and low hysteresis.

After 15 charge-discharge cycles, SEI films were observed on the surface of the GNS electrode. This can be seen in the SEM images (Figure 7). Apparently, the SEI films are made up of insoluble granular particles (Figure 7(b)), which arise from the decomposition of the electrolyte solvent. Figure 8 shows the XRD pattern of the GNS anode after being subjected to 15 charge-discharge cycles. After the charge-discharge cycles, GNS anode has features typical of expanded graphite [21,22], a weak (002) peak and a broader peak at 23–28°. This suggests that the stacking of

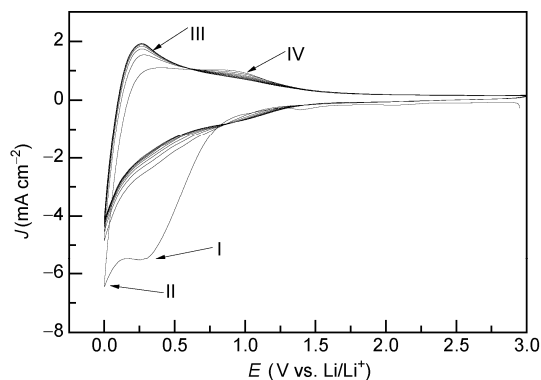


Figure 6 Cyclic voltammogram of the GNS anode in a three-electrode glass cell using Li foils as both counter and reference electrodes; scan rate: 1 mV s^{-1} .



Figure 7 SEM images of the GNS electrode after 15 charge-discharge cycles.

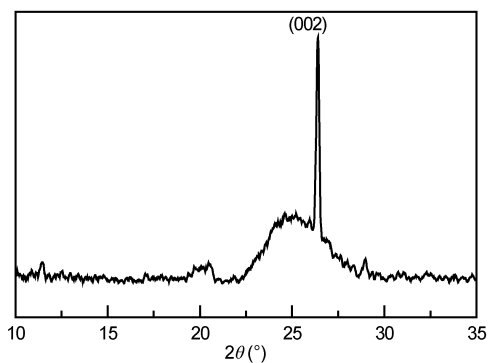


Figure 8 XRD pattern from the GNS electrode after 15 charge-discharge cycles.

graphene sheets is substantially disordered during the lithiation-delithiation cycles. This can also be confirmed through the SEM images (Figure 7 (a)).

2.4 EIS features of the GNS electrode

EIS spectra of the GNS electrode for different potentials during the first lithiation process are shown in Figures 9 and 10. The Nyquist plot of the GNS electrode at open circuit potential (OCP) (3.0 V) has a semicircle shape in the high-frequency (HF) range and is a slightly inclined line in the low-frequency (LF) region. This represents the blocking character of the nonlithiated electrode at the equilibrium potential [23]. Because there is not an initial SEI film on the

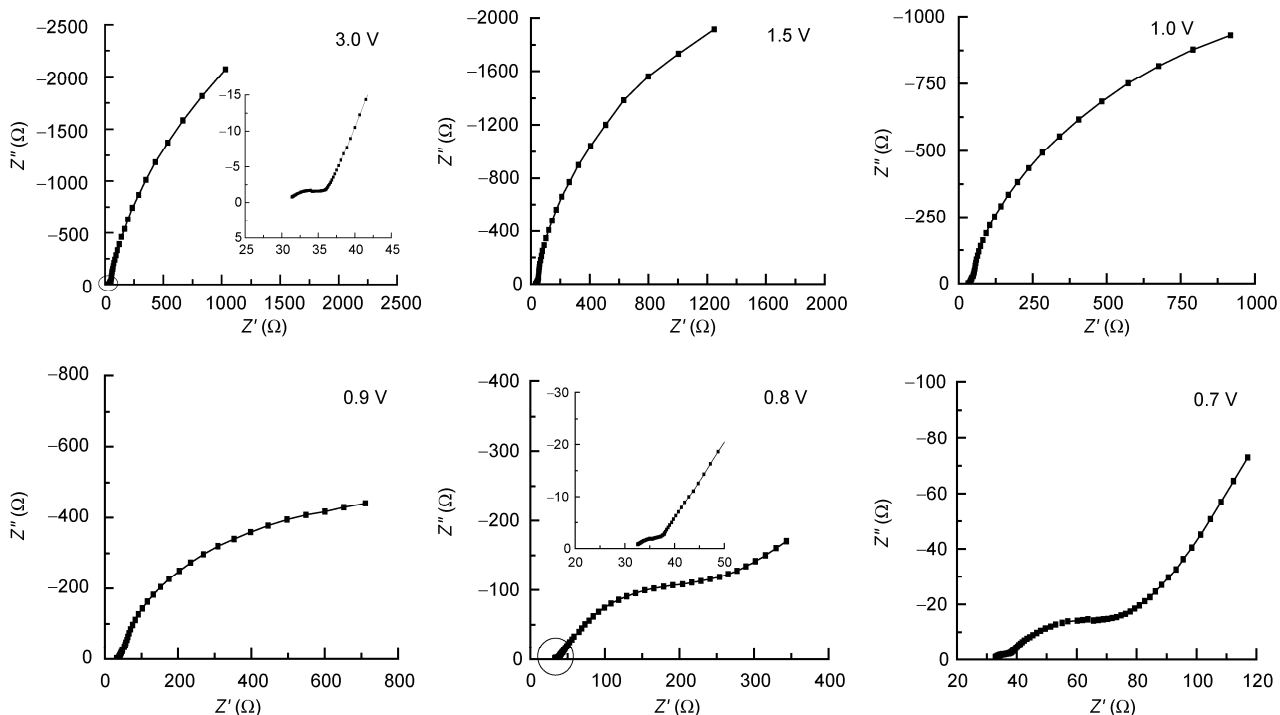


Figure 9 Nyquist plots for the GNS electrode at various potentials ranging from 3.0 to 0.7 V during the first lithiation over the frequency range 10^4 – 10^{-2} Hz.

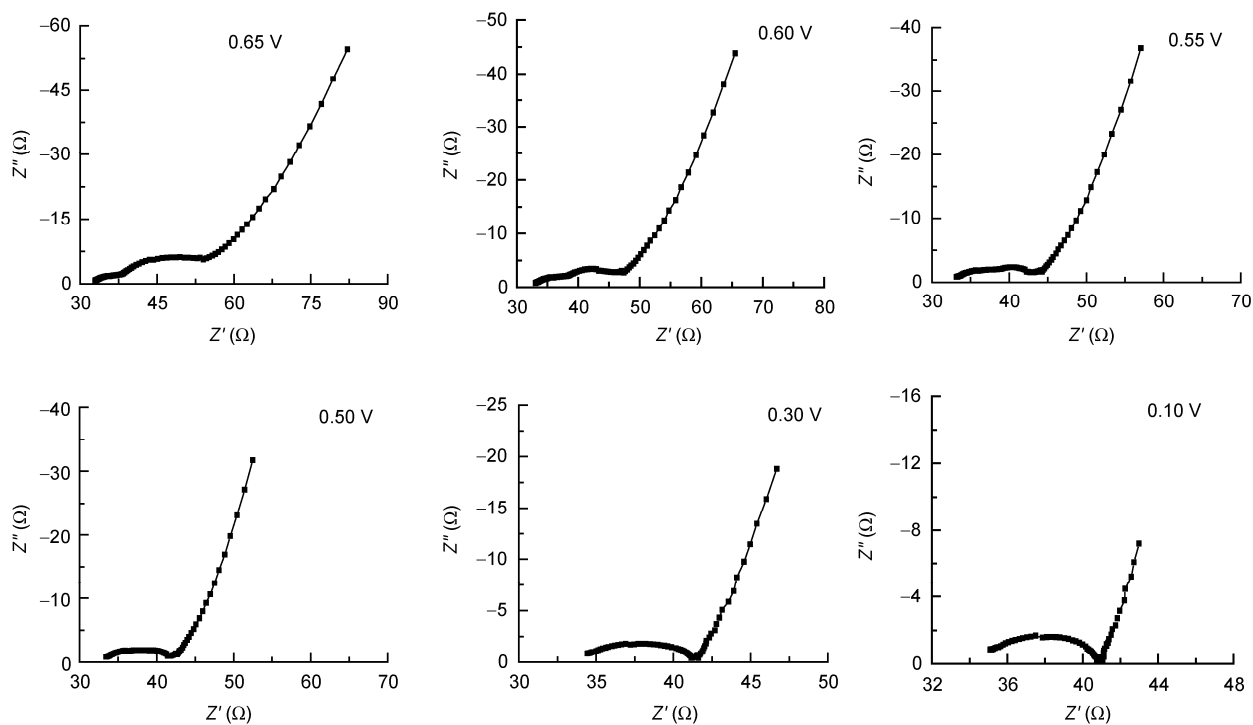


Figure 10 Nyquist plots for the GNS electrode at various potentials from 0.65 to 0.1 V during the first lithiation over the frequency range 10^4 – 10^{-2} Hz.

surface of GNSs or a formation process for SEI films at OCP, the semicircle in the high frequency region can be only attributed to contact problems, which was suggested by Holzapfel et al. [24].

The Nyquist plots above 1.0 V are similar to those at

OCP with a decreased electrode polarization potential. The similar features include a semicircular in the high frequency region and a line in the low frequency region. Also, there were no important modifications to the EIS traces in the high frequency region. These results illustrate that the

formation and growth of the SEI films, which are caused by electrolyte reduction decomposition, do not occur on the GNS electrode when the electrode polarization potential is above 1.0 V. This is in accordance with the CV results.

With decreasing electrode polarization potential, the inclined straight line, which is strongly potential dependent, moves closer towards the real axis. The plot becomes semi-circular in the medium-frequency (MF) region at 0.9 V. Also, a steep-slope line in the low frequency region is also formed at 0.8 V. In the region from 0.8 to 0.55 V, the Nyquist plots consist of three parts, two semicircles and one line. According to previous results for graphite electrodes [25–30], the HF semicircle is caused by lithium-ion migration through the SEI films, the MF semicircle can be attributed to the charge transfer step, and the steep-slope line is caused by solid state Li-ion diffusion in the bulk active mass. As previously mentioned, there is an initial semicircle in the high frequency region when the potential is above 1.0 V. Therefore, the HF semicircle observed in this study is not only related to the contact problems, but also lithium-ion migration through the SEI films. With the further decreases in electrode potential, the HF semicircle and the MF semicircle begin to overlap (below 0.5 V), and then totally merged into one single compressed semicircle (below 0.3 V).

2.5 Equivalent circuits proposed for EIS analysis

Based on the results obtained in this work, an equivalent circuit, which is shown in Figure 11, was proposed to match the impedance spectra of the GNS electrode during the first lithiation process. In this equivalent circuit, R_s represents the ohmic resistance, R_i is the resistance of the SEI films and/or the contact problems, R_{ct} is the resistance of the charge-transfer reaction. The capacitance of the SEI films and the capacitance of the double layer are represented using the constant phase elements (CPE) Q_1 and Q_{dl} , respectively. The low frequency region, however, cannot be modeled properly using a finite Warburg element. We chose, therefore, to replace the finite diffusion with a CPE, i.e. Q_D . This approach has been used to characterize graphite electrodes [31,32], and has allowed us to obtain a good match with the experimental data.

2.6 Variation in R_i with the electrode polarization potential

Figure 12 shows the variation in R_i with the electrode

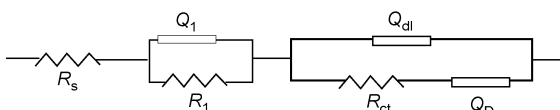


Figure 11 Equivalent circuit for the impedance spectra of the GNS electrode. R_s : ohmic resistance; R_i : resistances of the SEI and the contact problems; R_{ct} : charge-transfer resistance; Q_1 : SEI film capacitance; Q_{dl} : double layer capacitance; Q_D : diffusion capacitance.

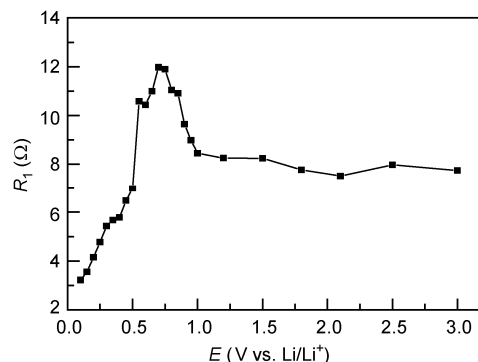


Figure 12 Variation in R_i with the electrode potential. This curve was obtained from fitting the experimental impedance spectra of the GNS electrode during the first charge-discharge cycle.

polarization potential. This was obtained by fitting the experimental impedance spectra from the GNS electrode during the first lithiation process. It can be seen that R_i remains fairly constant above 1.0 V. The value of R_i can be attributed to contact resistance, which was discussed above. When the electrode polarization potential decrease from 0.95 to 0.7 V, R_i rapidly increases. This corresponds to SEI film formation and the thickness of the newly formed SEI films. However, R_i quickly decreases with the decreasing electrode polarization potential below 0.7 V. This may be caused by the volume increase in the graphene sheets increases associated with lithium-ion intercalation. This improves contact among the graphene sheets and between the current collector and the graphene sheets, which leads to a decrease in R_i .

2.7 Variation in charge transfer resistance with electrode polarization potential

The basic reaction mechanism of lithium-ion intercalation in the GNS electrode is represented by eq. (1):



First, assume that the velocity of the forward reaction r_f (lithium-ion intercalation in the GNS electrode) is proportional to $c_T(1-x)$ and the concentration (M^+) of lithium-ions in the electrolyte near the electrode. $c_T(1-x)$ is the concentration of intercalation sites on the GNS electrode surface unoccupied by lithium-ions, x is the intercalation level, c_T (mol cm^{-3}) is the maximum concentration of lithium-ions in GNS electrode. Then, the deintercalation rate, r_b , is proportional to $c_T x$, which represents the lithium-ion sites. Therefore the intercalation velocity, r_f , and the deintercalation velocity, r_b , can be expressed as [33]:

$$r_f = k_f c_T (1-x) M^+, \quad (2)$$

$$r_b = k_b c_T x. \quad (3)$$

Therefore:

$$i = r_f - r_b = nF c_T [k_f (1-x) M^+ - k_b x], \quad (4)$$

where n is the number of electron exchanges during charging and discharging, and F is the Faraday constant.

The molar intercalation energy, ΔG_{int} , of lithium-ions in the GNS electrode can be expressed as:

$$\Delta G_{\text{int}} = a + gx, \quad (5)$$

where a is the interaction energy between an intercalated ion and a host lattice near it, and g is the interaction energy between two intercalated ions at different sites.

According to activated complex theory:

$$k_f = k_f^0 \exp\left[\frac{-\alpha(nFE + \Delta G_{\text{int}})}{RT}\right], \quad (6)$$

$$k_b = k_b^0 \exp\left[\frac{(1-\alpha)(nFE + \Delta G_{\text{int}})}{RT}\right], \quad (7)$$

where α is the symmetry factor for the electrochemical reaction. The velocity constants, k_f^0 and k_b^0 , can be expressed in the Arrhenius form [34]:

$$k_f^0 = A_f \exp\left(\frac{-\Delta G_{0c}}{RT}\right), \quad (8)$$

$$k_b^0 = A_b \exp\left(\frac{-\Delta G_{0a}}{RT}\right). \quad (9)$$

Substituting eqs. (6) and (7) into eq. (4), the current, i , can be obtained from the following expression:

$$i = nFc_T k_f^0 (1-x) M^+ \exp\left[\frac{-\alpha(nFE + \Delta G_{\text{int}})}{RT}\right] - nFc_T k_b^0 x \exp\left[\frac{(1-\alpha)(nFE + \Delta G_{\text{int}})}{RT}\right]. \quad (10)$$

For the equilibrium state, $E = E_c$ and $i = 0$. Therefore, the exchange current density, i_0 , can be expressed as:

$$i_0 = nFc_T k_f^0 (1-x) M^+ \exp\left[\frac{-\alpha(nFE + \Delta G_{\text{int}})}{RT}\right] = nFc_T k_b^0 x \exp\left[\frac{(1-\alpha)(nFE + \Delta G_{\text{int}})}{RT}\right]. \quad (11)$$

Thus:

$$i_0 = nFc_T k_0 (M^+)^{(1-\alpha)} (1-x)^{(1-\alpha)} x^\alpha, \quad (12)$$

where k_0 is the standard reaction speed constant, and k_0 can be expressed as:

$$k_0 = k_f^0 \exp\left[\frac{-\alpha(nFE_0 + \Delta G_{\text{int}})}{RT}\right] = k_b^0 \exp\left[\frac{(1-\alpha)(nFE_0 + \Delta G_{\text{int}})}{RT}\right]. \quad (13)$$

The charge transfer resistance can be defined as:

$$R_{\text{ct}} = RT/nFi_0. \quad (14)$$

Substituting eqs. (10) and (12) into eq. (14) gives the following formula:

$$R_{\text{ct}} = \frac{RT}{n^2 F^2 C_T k_0 (M^+)^{(1-\alpha)} (1-x)^{(1-\alpha)} x^\alpha}. \quad (15)$$

If the reactions of lithium-ion intercalation and deintercalation in the GNS electrode are invertible, α will be equal to 0.5. Then:

$$R_{\text{ct}} = \frac{RT}{n^2 F^2 C_T k_0 (M^+)^{0.5} (1-x)^{0.5} x^{0.5}}. \quad (16)$$

Equation (16) predicts a rapid increase in R_{ct} with the decreasing x for $x < 0.5$, and a rapid decrease in R_{ct} with increasing of x for $x > 0.5$. The minimum R_{ct} can be attained when $x = 0.5$. Equation (16) can explain the relation between the charge-transfer resistance and the electrode polarization potential. This is shown in Figure 13.

If the interaction between intercalated lithium ions at different sites and the interaction between intercalated lithium ions and the host lattice near are neglected, a Langmuir type isotherm can be used to describe lithium insertion-extraction into GNS electrode. In this case, the relationship between the insertion level, x , and the electrode polarization potential has the following form [35]:

$$x/(1-x) = \exp[f(E - E_0)], \quad (17)$$

Where $f = F/RT$; R and F are the thermodynamic and Faraday constants, respectively; E and E_0 are the electrode's real and standard potentials, respectively.

Initially, a lithium ion is inserted into or extracted from the active mass during the electrochemical processes. That is to say, for a very low insertion level ($x \rightarrow 0$). Equation (17) takes the form:

$$x = \exp[f(E - E_0)]. \quad (18)$$

After substituting eq. (18) into eq. (16), R_{ct} can be rewritten as:

$$R_{\text{ct}} = \frac{RT}{n^2 F^2 C_T k_0 (M^+)^{(1-\alpha)} \exp[-\alpha f(E - E_0)]}. \quad (19)$$

By linearizing eq. (19) using a logarithm, we obtain the following expression:

$$\ln R_{\text{ct}} = \ln \frac{RT}{n^2 F^2 C_T k_0 (M^+)^{(1-\alpha)}} - \alpha f(E - E_0). \quad (20)$$

Equation (20) indicates that, if $x \rightarrow 0$, $\ln R_{\text{ct}}$ and E has a linear variation. The symmetry factor α can be obtained from the slope. Figure 13(b) shows the variation in $\ln R_{\text{ct}}$ with electrode

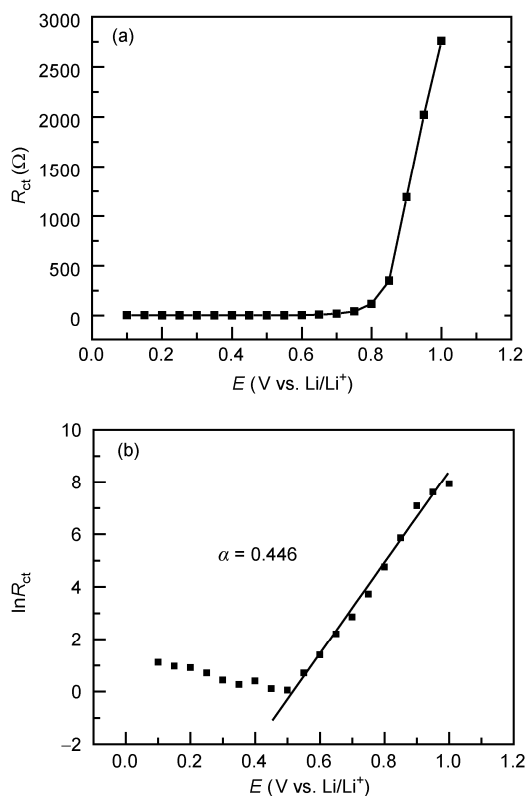


Figure 13 Variations in R_{ct} and $\ln(R_{ct})$ with the electrode polarization potential obtained from fitting the experimental impedance spectra of the GNS electrode during the first lithiation.

polarization potential, which was obtained by fitting the experimental impedance spectra of the GNS electrode. From this, it can be seen that eq. (20) can be used to properly interpret the experimental data. $\ln R_{ct}$ varies linearly with the electrode polarization potentials between 0.5 and 1.0 V during the first lithium-ion intercalation process and a value of 0.446 for α can be calculated using the slope of the line in Figure 13 (b).

3 Conclusions

In summary, GNSs were synthesized by reducing exfoliated graphite oxides. It was found that, GNSs were primarily few-layer graphene sheets with less than 10 layers. We fabricated GNS electrodes that exhibited an enhanced reversible lithium storage capacity and good cyclic stability when serving as anodes in lithium-ion batteries. Also, the first-cycle irreversible capacities were relatively high, because of the formation of solid electrolyte interphase films on the surface of the GNS electrodes and the spontaneous stacking of GNSs during the first lithiation. The EIS results suggest that the SEI films that formed on GNS electrodes during first lithiation did so at potential values between 0.7–0.95 V. We also measured the symmetry factor of the charge transfer to be 0.446.

The authors are grateful for assistance with SEM, AFM and XRD measurements from Prof. Ding ShiJin and Lan Lan from the School of Microelectronics, Fudan University. This work was supported by the Fundamental Research Funds for the Central Universities (2010LKH03, 2010QNB04, 2010QNB05), the Science and Technology "Climbing" Program of China University of Mining & Technology (ON090237).

- Novoselov K S, Geim A K, Morozov S V, et al. Electric field effect in atomically thin carbon films. *Science*, 2004, 306: 666–669
- Geim A K, Novoselov K S. The rise of graphene. *Nat Mater*, 2007, 6: 183–191
- Novoselov K S, Geim A K, Morozov S V, et al. Two-dimensional gas of massless Dirac fermions in graphene. *Nature*, 2005, 438: 197–200
- Hernandez Y, Nicolosi V, Lotya M, et al. High-yield production of graphene by liquid-phase exfoliation of graphite. *Nat Nanotech*, 2008, 3: 563–568
- Banhart F, Ajayan P M. Carbon onions as nanoscopic pressure cells for diamond formation. *Nature*, 1996, 382: 433–435
- Chae H K, Siberio Perez D Y, Kim J, et al. A route to high surface area, porosity and inclusion of large molecules in crystals. *Nature*, 2004, 427: 523–527
- Wang Y, Huang Y, Song Y, et al. Room temperature ferromagnetism of graphene. *Nano Lett*, 2009, 9: 220–224
- Chen J H, Jang C, Xiao S D, et al. Intrinsic and extrinsic performance limits of graphene devices on SiO_2 . *Nat Nanotech*, 2008, 3: 206–209
- Partoens B, Peeters F M. From graphene to graphite: Electronic structure around the K point. *Phys Rev B*, 2006, 74: 075404
- Rao C N R, Sood A K, Subrahmanyam K S, et al. Graphene: The new two-dimensional nanomaterial. *Angew Chem Int Ed*, 2009, 48: 7752–7778
- Wang G X, Shen X P, Yao J, et al. Graphene nanosheets for enhanced lithium storage in lithium ion batteries. *Carbon*, 2009, 47: 2049–2053
- Yoo E J, Kim J, Hosono E, et al. Large reversible Li storage of graphene nanosheet families for use in rechargeable lithium ion batteries. *Nano Lett*, 2008, 8: 2277–2282
- Hummers W S, Offeman R E. Preparation of graphitic oxide. *J Am Chem Soc*, 1958, 80: 1339
- Stankovich S, Dikin D A, Piner R D, et al. Synthesis of graphene-based nanosheets via chemical reduction of exfoliated graphite oxide. *Carbon*, 2007, 45: 1558–1565
- Guo P, Song H, Chen X. Electrochemical performance of graphene nanosheets as anode material for lithium-ion batteries. *Electrochem Commun*, 2009, 11: 1320–1324
- Wang C, Li Dan, Too C O, et al. Electrochemical properties of graphene paper electrodes used in lithium batteries. *Chem Mater*, 2009, 21: 2604–2606
- Schniepp H C, Li J L, McAllister M J, et al. Functionalized single graphene sheets derived from splitting graphite oxide. *J Phys Chem B*, 2006, 110: 8535–8539
- Zhuang Q C, Tian L L, Wei G Z, et al. Two- and three-electrode impedance spectroscopic studies of graphite electrode in the first lithiation. *Chinese Sci Bull*, 2009, 54: 2627–2632
- Zhuang Q C, Chen Z F, Dong Q F, et al. Effects of methanol contaminant in electrolyte on performance of graphite electrodes for Li-ion batteries studied via electrochemical impedance spectroscopy (in Chinese). *Chem J Chinese Univ*, 2005, 26: 2073–2076
- Pan D Y, Wang S, Zhao B, et al. Li storage properties of disordered graphene nanosheets. *Chem Mater*, 2009, 21: 3136–3142
- Wu Z S, Ren W, Gao L, et al. Synthesis of graphene sheets with high electrical conductivity and good thermal stability by hydrogen arc discharge exfoliation. *ACS Nano*, 2009, 3: 411–417
- Falcao E H L, Blair R G, Mack J J, et al. Microwave exfoliation of a graphite intercalation compound. *Carbon*, 2007, 45: 1364–1369
- Chang Y C, Sohn H J. Electrochemical impedance analysis for lithium ion intercalation into graphite carbons. *J Electrochem Soc*, 2000, 147: 50–58
- Holzappel M, Martinet A, Allion F, et al. First lithiation and charge/discharge cycles of graphite materials, investigated by electrochem-

- ical impedance spectroscopy. *J Electroanal Chem*, 2003, 546: 41–50
- 25 Levi M D, Aurbach D. Distinction between energetic in homogeneity and geometric non-uniformity of ion insertion electrodes based on complex impedance and complex capacitance analysis. *J Phys Chem B*, 2005, 109: 2763–2773
- 26 Levi M D, Aurbach D. Simultaneous measurements and modeling of the electrochemical impedance and the cyclic voltammetric characteristics of graphite electrodes doped with lithium. *J Phys Chem B*, 1997, 101: 4630–4640
- 27 Aurbach D, Levi M D, Levi E, et al. Common electroanalytical behavior of Li intercalation processes into graphite and transition metal oxides. *J Electrochem Soc*, 1998, 145: 3024–3034
- 28 Aurbach D, Gamolsky K, Markovsky B, et al. The study of surface phenomena related to electrochemical lithium intercalation into Li_xMO_y host materials ($M = \text{Ni}, \text{Mn}$). *J Electrochem Soc*, 2000, 147: 1322–1331
- 29 Markovsky B, Levi M D, Aurbach D. The basic electroanalytical behavior of practical graphite-lithium intercalation electrodes. *Electrochim Acta*, 1998, 43: 2287–2304
- 30 Aurbach D. Review of selected electrode-solution interactions which determine the performance of Li and Li ion batteries. *J Power Sources*, 2000, 89: 206–218
- 31 Zhuang Q C, Chen Z F, Dong Q F, et al. Studies of the first lithiation of graphite materials by electrochemical impedance spectroscopy. *Chinese Sci Bull*, 2006, 51: 17–20
- 32 Zhang S, Shi P. Electrochemical impedance study of lithium intercalation into MCMB electrode in a gel electrolyte. *Electrochim Acta*, 2004, 49: 1475–1482
- 33 Barrel G, Diard J P, Montella C. Etude d'un modele de reaction electrochimique d'insertion-i. Resolution pour une commande dynamique a petit signal. *Electrochim Acta*, 1984, 29: 239–246
- 34 Li Y, Wu H. Theoretical treatment of kinetics of intercalation electrode reaction. *Electrochim Acta*, 1989, 34: 157–159
- 35 Levi M D, Aurbach D. Frumkin intercalation isotherm — a tool for the description of lithium insertion into host materials: A review. *Electrochim Acta*, 1999, 45: 167–185

Open Access This article is distributed under the terms of the Creative Commons Attribution License which permits any use, distribution, and reproduction in any medium, provided the original author(s) and source are credited.